Conformational Entropy as a Means to Control the Behavior of Poly(diketonenamine) Vitrimers In and Out of Equilibrium

Changfei He,[1] Peter R. Christensen,[2] Trevor J. Seguin,[3] Brandon M. Wood,[4,5] Kristin A. Persson,[5,6] Thomas P. Russell,[*,1,7,8] and Brett A. Helms[*,2,8]

[1]Beijing Advanced Innovation Center for Soft Matter Science and Engineering, Beijing University of Chemical Technology, Beijing 100029, China

[2]The Molecular Foundry, Lawrence Berkeley National Laboratory, 1 Cyclotron Road, Berkeley, California 94720, United States

[3]Energy Technologies Area, Lawrence Berkeley National Laboratory, 1 Cyclotron Road, Berkeley, California 94720, United States

[4]Graduate Group of Applied Science and Technology, University of California, Berkeley, California 94720, United States

[5]Environmental Energy Technologies Division, Lawrence Berkeley National Laboratory, 1 Cyclotron Road, Berkeley, California 94720, United States

[6]Materials Science and Engineering Department, University of California, Berkeley, California 94720, United States

[7]Polymer Science and Engineering Department, University of Massachusetts Amherst, Massachusetts 01003, United States

[8]Materials Sciences Division, Lawrence Berkeley National Laboratory, 1 Cyclotron Road, Berkeley, California 94720, United States

Supporting Information Placeholder

ABSTRACT: Here we show how to control the thermomechanical behavior of vitrimers, both in and out of equilibrium, by incorporating into the dynamic covalent network linear polymer segments varying in both molecular weight (MW = 0–12 kg mol^{-1}) and conformational degrees of freedom. While increasing MW of linear segments predictably yields a lower storage modulus (E') at the rubbery plateau after softening above the glass transition (T_g), due to the lower network density, we further find that both T_g and the characteristic time (τ^*) of stress-relaxation when deformed are independently governed by the conformational entropy of the embodied linear segments. We also find that activation energies (E_a) for vitrimer bond exchange in the solid-state are lower, by as much as 19 kJ mol^{-1}, for networks incorporating flexible chains, and that the network's topology freezing temperature (T_v) decreases with increasing MW of flexible linear segments, but increases with increasing MW of stiff linear segments. Therefore, the dynamics of vitrimer reconfigurability are influenced not only by the energetics of associative bond exchange for a given network density, but also foundationally by the entropy of polymer chains within the network.

Vitrimers are living polymer networks that reconfigure via dynamic associative bond-exchange reactions, laying the foundations for both self-healing plastics and post-industrial plastics recycling.[1–3] A vitrimer's cross-linking density influences its thermal and mechanical properties: e.g., higher network density increases the probability that cross-links will interact and be involved in bond-exchange reactions, which impact the dynamics of vitrimer reconfigurability across multiple length scales and therefore its rheology. The energetics of bond-exchange reactions have been studied for vitrimers undergoing uncatalyzed and catalyzed transesterification,[4–6] transcarbamoylation,[7–10] olefin metathesis,[11] boronic ester exchange,[12–14] siloxane exchange,[15,16] triazolium transalkylation,[17] imine bond exchange,[18,19] ketoenamine exchange,[20–22] and diketoenamine exchange[23]. However, there is a lack of understanding of how conformational degrees of freedom available to the network influence a vitrimer's thermal and rheological behavior in and out of equilibrium.

Here, we show that the incorporation of conformationally flexible or, alternatively, stiff ditopic (A2) monomers into a vitrimer network otherwise comprised of tritopic (A3) and ditopic B2 monomers allows the network density to be independently modulated from the network's thermal, mechanical, and rheological properties. We exerted fine-control over such architectural attributes in a vitrimer using poly(diketoenamine)s, or PDKs, which "click" together via spontaneous condensation reactions between polytopic triketone and amine monomers (Figure 1a).[23] PDK **1**, which exhibits the highest network density, was generated from ditopic triketone monomer TK-10 and tris(aminoethyl)amine (TREN) as the crosslinker (Scheme 2). We also introduced to PDK **1** linear segments of varying molecular weight with conformational degrees of freedom by adding either trimethylhexamethylene diamine (TMHDA) or isophorone diamine (IPDA) in controlled amounts (20–60 mol%) to the reaction mixture (Figure 1c). Torsional partition functions, q_{tor}, for TMHDA- and IPDA-based monomer segments differentiate each monomer by conformational degrees of freedom; by extension, linear PDK segments incorporating TMHDA and IPDA are

comparably flexible or stiff, respectively (Figure 1b). THMDA, IPDA, and dimedone-derived TK monomers each originate from acetone as a common starting material, which is available by microbial fermentation, suggesting bio-sourced feedstocks for recyclable PDK vitrimers with controlled properties are in reach.[24–26]

To synthesize this family of PDK vitrimers—where PDKs **2**–**4** incorporate 20, 40, and 60 mol% TMHDA, and PDKs **5**–**7** incorporate 20, 40, and 60 mol% IPDA—the linear segments for diamine-modified PDK vitrimers were initially synthesized in the melt from ditopic triketone TK-10 and either of the diamines prior to introducing TREN to crosslink the networks. This ensured that the gel fractions were in excess of 95% to the differentiated reactivity (i.e., sterics) of the various amines in the monomer feed (Table S1). We did not advance to higher diamine content than 60%, as we would have eventually hit the limit for the gel point in polymer networks for mixtures of ditopic and tritopic amine monomers (~74 mol% diamine relative to triamine for a 10% total amine excess relative to triketones from ditopic TK-10).

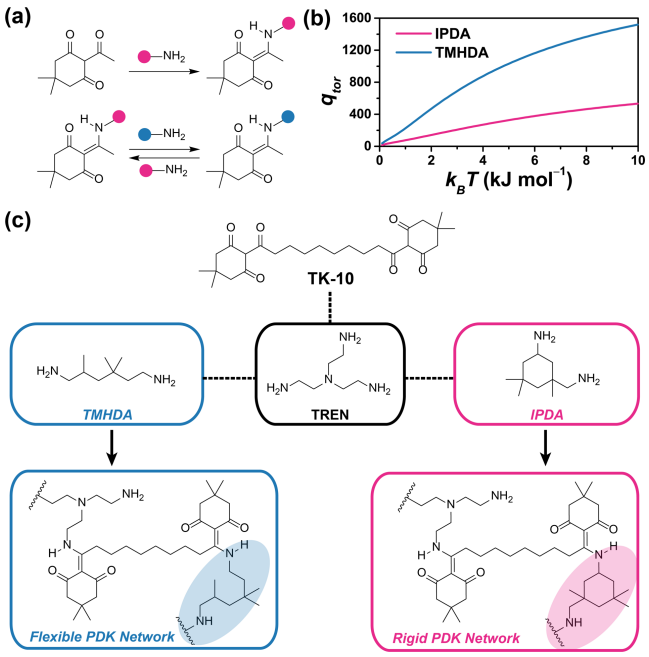

Figure 1. (a) Triketones and amines self-condense to yield dynamic covalent diketoenamines, which undergo bond exchange reactions with amines. (b) Partition functions differentiating the conformational degrees of freedom for TMHDA- and IPDA-based small molecule models of the microstructural elements in PDK vitrimers **2**–**7**. (c) Synthesis of PDK vitrimers **1**–**7** via clickable polycondensation reactions.

Homogeneous distribution of TMHDA and IPDA diamines in PDKs **2**–**7** is evidenced from the linearity of T_g^{-1} (determined by differential scanning calorimetry, DSC) as a function of the diamine content, which are related by the Flory–Fox equation (Figure S2 and Figure 2a);[27] PDK vitrimers incorporating only TK-10 and TREN, as well as linear PDK polymers synthesized from TK-10 and either TMHDA or IPDA and TK-10, provided the end-points for the comprehensive analysis. Notably, the incorporation of flexible TMHDA-based linear segments decreased T_g relative to the parent PDK network incorporating only TREN, while the incorporation of stiff IPDA-derived linear segments increased T_g; each dependency manifested in a well-behaved manner, albeit divergent. Accordingly, the predictability with which one may tune T_g in PDKs due to the ease in which homogeneous network architectures are available suggests advantages over other network polymers where chemical heterogeneity is unavoidable, as is the case with many conventional thermosets and some thermally reprocessable thermosets based on other vitrimer chemistries. On account of their homogeneity, it also becomes possible to directly tie their emergent thermomechanical behaviors to well-defined vitrimer architectures.

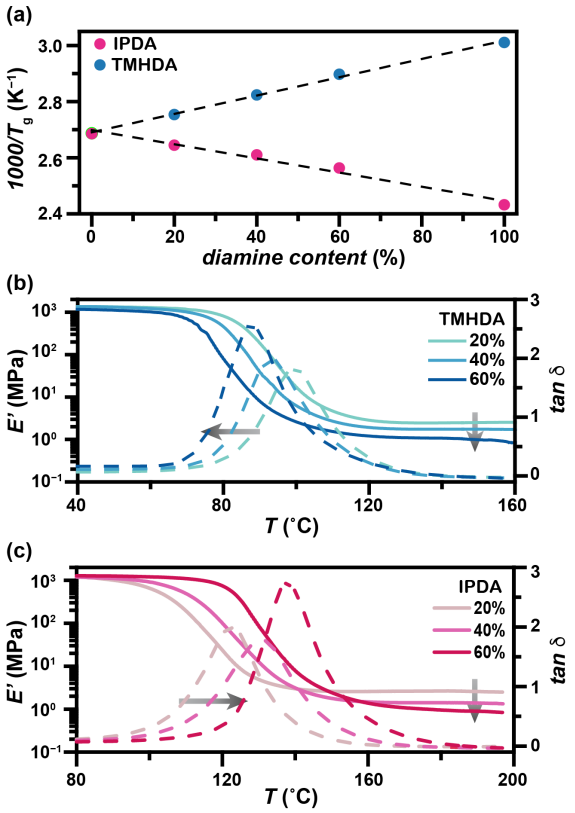

Figure 2. (a) Flory–Fox analysis of PDK vitrimers **1**–**7** and linear polymers derived from TK-10 and either TMHDA or IPDA. (b) Temperature-Dependent storage modulus (*E'*) and tan δ for TMHDA-based PDK vitrimers **2**–**4** (b), and IPDA-based vitrimers **5**–**7** (c).

To characterize the range of embodied architectural attributes of TMHDA- and IPDA-modified PDK networks, we carried out extensive dynamic mechanical analyses (DMA) (Figure 2 and Tables S2–4), which indicated ambient temperature storage moduli of *E'* = 1.4–2.0 GPa (Figure 2b,c) as well as tensile strengths of σ = 18.5–30 MPa (Table S4), which are similar to many epoxies.[28] Furthermore, once heated above their T_g, each PDK's storage modulus in the rubbery plateau was then used to estimate PDK crosslinking density (ν), and in turn the *MW* of diamine-derived linear segments between TREN-derived cross-linking points (Table S2): here, such segments varied 3.8–9.6 kg mol^{-1} for THMDA loadings of 20–60%; similarly, 4.0–11.0 kg mol^{-1} for IPDA loadings of 20–60%. These data also provided independent determination of T_g (from the maximum in *tan* δ) and in turn provided support for our hypothesis that the softening temperature in vitrimers is not only dictated by the *MW* of the polymer chains between crosslinks, but also the conformational degrees of freedom available to those chains in the network.

The rheological properties of PDK vitrimers underlie their prospects for both polymer processing during manufacturing, their mechanical response to deformation, their ageing mechanisms while in service, and their prospects for scrap recovery via remolding and reuse (i.e., post-industrial recycling); we provide details regarding post-industrial PDK recycling in the Supporting Information (Figure S3). To begin unpacking the differentiated rheological characteristics of PDK vitrimers **2**–**7**, we conducted a series of stress-relaxation experiments whereby a strain of 1% (within the linear viscoelastic regime) was applied to compression-molded PDK samples, and the ensuing stress decay was then monitored as a function of time. As is typical for vitrimers, complete relaxation was observed after the application of strain over the entire temperature range due to diketoenamine bond-exchange reactions. The characteristic stress-relaxation time (τ^*) is determined at ratio of e^{-1} with regard to the relaxation modulus (G) relative to the initial (G_0). We found that increasing the diamine content in PDK vitrimers resulted shorter τ^* values: for example, at T = 150 ˚C, τ^* decreased from 151 s to 81 s with an increase in the TMHDA content from 20% to 60%. Since higher diamine-content vitrimers have lower moduli at the rubbery plateau, PDKs yield lower viscosity at the same temperature, i.e., the active chain ends can redistribute more freely in the network. However, we also observed by comparing TMHDA- and IPDA-based vitrimers having the same diamine content (e.g., 40%) at the same temperature (e.g., T = 150 ˚C) that τ^* was considerably shorter for PDK networks with higher conformational entropy: e.g., τ^* = 110 s for TMHDA-based PDK **3** with 6.3 kg mol^{-1} linear segments, compared to τ^* = 457 s for PDK **6** with 7.8 kg mol^{-1} linear segments. IPDA-based PDKs consistently yield lower viscosity than TMHDA-based vitrimers for an equivalent diamine loading when interrogated at the same temperature, i.e., the active chain ends in IPDA-based vitrimers do not redistribute as freely in the network as do those in TMHDA-based vitrimers. This confirms our hypothesis that conformational entropy dictates the rheological behavior of PDK vitrimers for a given *MW* of linear segments in the network (Figure 3a,b and Figure S4).

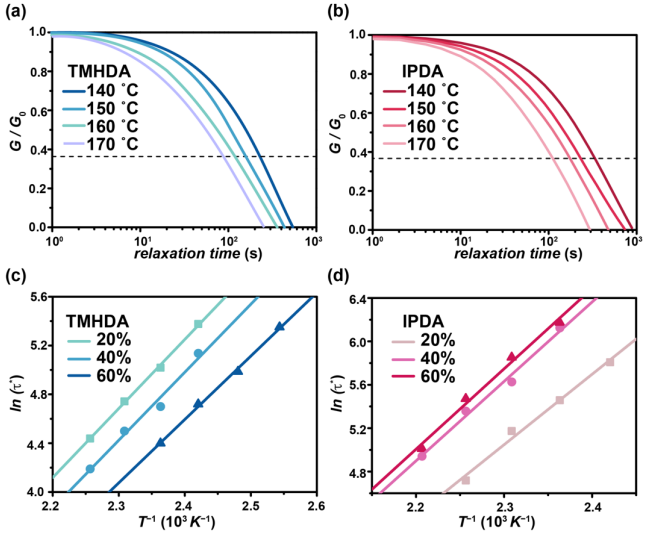

Figure 3. Normalized stress-relaxation curves at different temperatures for PDKs (a) **2** (20% TMHDA) and (b) **5** (20% IPDA). Dashed lines indicate 37% of G_0. Data were acquired at 1% strain. Arrhenius plots relating τ_0 to T^{-1} for PDKs **2**–**7**.

While we were able to glean key differences in the dynamic behavior associated with stress relaxation for PDK networks incorporating flexible and stiff linear segments, we were further able to assess the impact of these polymer network architectures on the activation barriers to diketoenamine bond exchange in the solid-state. Here, Arrhenius behavior governs the rheological properties of PDK networks, as viscoelastic flow requires a series of bond exchange events in order for the network to return to equilibrium after the application of strain. For TMHDA loadings of 20–60%, we observed E_a values of 47±1.3, 46±4.4, and 43±1.5 kJ mol^{-1}; for IPDA loadings of 20–60% we observed E_a values of 54±4.1, 60±4.3, and 62±4.4 kJ mol^{-1}. In general, E_a values reflect a convolution of: 1) stereoelectronics associated with the different types of amine exchange reactions that can proceed with the available electrophiles, and 2) entropic penalties associated with deforming chains, particularly when they are stiff, as is the case for IPDA-derived linear segments. Comparing E_a for TMHDA- and IPDA-based PDK networks, each at 20% loading, the difference can be as high as 19 kJ mol^{-1}. Thus, while there has been extensive effort to understand differences in E_a for bond exchange reactions for small molecule vitrimer analogs in solution and for fully formed vitrimers in the solid-state, only now have we discerned that for architecturally similar vitrimers, microstructural differences in the monomer constituents play the dominant role in the observed materials properties, both in and out of equilibrium. Moreover, this dynamic behavior appears to be controllable at the level of monomers, as these choices set forth the energy landscapes available to the system to reconfigure.

We further evaluated the impact of network microstructure on how PDK vitrimers flow for architecturally similar networks by determining, via the Maxwell relation, the topology freezing transition temperature (T_v), which relates the temperature at which the vitrimer's viscosity increases above $\eta = 10^{12}$ Pa s. For all PDK vitrimers, $T_v < T_g$, indicating that the topology of network remains frozen below T_g even though bond exchange reactions are, in principle, allowed. It is further notable that T_v decreased from −20 ˚C to −45 ˚C as the TMHDA loading was increased from 20% to 60%, whereas it increased from −1 °C to 11 ˚C as the IPDA loading was increased from 20% to 60% (Table S3). This indicates that the softer TMHDA-derived linear segments of allow the network to flow more easily, while the more rigid IPDA-derived linear segments make flow more difficult.

Toward a molecular understanding of how TMHDA and IPDA exert their distinctive influence on the rheological properties of PDKs, we computationally explored the conformational degrees of freedom of each species by scanning the torsional potential of bonds involved, which are highly differentiated in their flexibilities. We also computed the corresponding torsional partition functions q_{tor}. The torsional potential scans were performed by rotating a bond 360 degrees and allowing the remainder of the molecule to relax. Conformation searches were performed to obtain the global minimum energy conformations to be used as starting points, and further conformation searches were carried out at intermediate steps of the scans to ensure full relaxation of the molecule outside of the bond involved in the scan (see Supporting Information). The torsional potential of all of the rotating bonds for TMHDA and IPDA were examined: bonds B1–7 and bonds B1–3, respectively (Figure 4, insets). The partition functions q_{tor} provide a sense of the number of states thermally accessible to each species by torsional rotation. These quantities for TMHDA- and IPDA-based monomer segments are presented in Figure 1b, and their ratio in Figure S6. Segments based on TMHDA possess a greater number of accessible states up to 10 k_BT. This difference in accessible states is related, in part, to the difference in the number of rotatable bonds, but also the

energy landscapes for bond rotation, which are chemistry-specific. For example, strictly considering the number of bonds and not the chemistry of each monomer segment, a ratio of 7/3 (≈ 2.33) would be expected. However, the calculations show q(THMDA)/q(IPDA) are higher across the range of k_BT, highlighting the critical role of monomer segment's embodied chemistry. This ratio reaches a maximum of 3.33 near $2k_BT$, and decreases at higher k_BT as more of the conformational states become accessible to the IPDA segments (Figure S6). This fundamental difference in flexibility gives rise to the differences observed rheological properties at elevated temperature of PDKs that incorporate microstructural elements with varying conformational entropy.

Microstructural and architectural attributes of PDK vitrimers (and likely others) therefore emerge as powerful elements of design for controlling the thermomechanical behavior of vitrimers in and out of equilibrium, with respect to the bond exchange reactions foundational to their reconfigurability and the conformational entropy of polymer chains in the network. Entropic and stereoelectronic considerations can result in divergent energetics to bond exchange in the solid-state by as much as 19 kJ mol^{-1} for architecturally similar networks incorporating chains with varying conformational degrees of freedom, or structure of nucleophilic amine and electrophilic diketoenamine partners. We further see controllably divergent dependencies for both T_g and T_v with flexible and stiff diamine monomers, highlighting the distinctive role played by microstructure on these characteristics. Their influence on vitrimer dynamics cannot be understated and suggest exciting paths forward for controlling vitrimer processing.

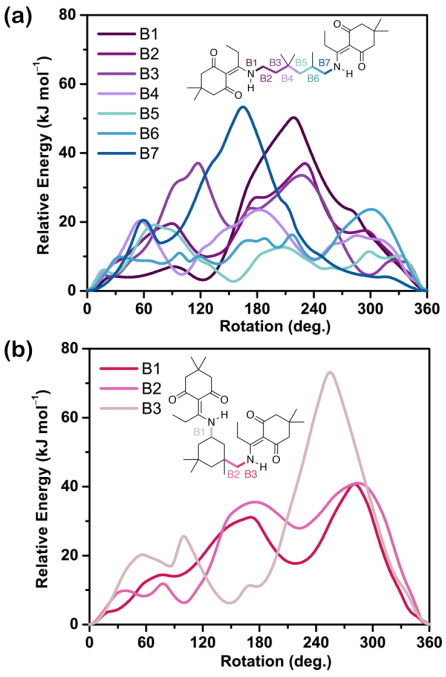

Figure 4. Torsional strain energies for various bonds in model compounds representing TMHDA-based (a) and IPDA-based (b) PDK monomer segments.

ASSOCIATED CONTENT

Supporting Information

The Supporting Information is available free of charge on the ACS Publications website. Supporting Methods, Supporting Figures S1–S6, and Supporting Tables S1–S4.

AUTHOR INFORMATION

Corresponding Author

tom.p.russell@gmail.com; bahelms@lbl.gov.

Notes

The authors declare the following competing interests: BAH and PRC are inventors on US provisional patent application 62/587,148 submitted by Lawrence Berkeley National Laboratory that covers poly(diketoenamine)s, as well as aspects of their use and recovery.

ACKNOWLEDGMENT

The technical scope of work was supported by the Laboratory Directed Research and Development Program of Lawrence Berkeley National Laboratory under U.S. Department of Energy Contract No. DE-AC02-05CH11231. Portions of this work, including organic and polymer synthesis and characterization, were carried out as a User Project at the Molecular Foundry, which is supported by the Office of Science, Office of Basic Energy Sciences, of the U.S. Department of Energy under the same contract. Computational resources were provided by the Savio cluster of the Berkeley Research Computing program at the University of California, Berkeley. The computational effort was partially supported by the Joint Center for Energy Storage Research (JCESR), an Energy Innovation Hub funded by the U.S. Department of Energy, Office of Science, Office of Basic Energy Sciences (BES).

REFERENCES

(1) Montarnal, D.; Capelot, M.; Tournilhac, F.; Leibler, L. *Science* **2011**, *334*, 965–968.
(2) Denissen, W.; Winne, J. M.; Du Prez, F. E. *Chem. Sci.* **2016**, *7*, 30–38.
(3) Fortman, D. J.; Brutman, J. P.; De Hoe, G. X.; Snyder, R. L.; Dichtel, W. R.; Hillmyer, M. A. *ACS Sus. Chem. Eng.* **2018**, *6*, 11145–11159.
(4) Brutman, J.; Delgado, A.; Hillmyer, M. *ACS Macro Lett.* **2014**, *3*, 607–610.
(5) Zhou, Y.; Goossens, J. P.; Sijbesma, R.; Heuts, J. A. *Macromolecules* **2017**, *50*, 6742–6751.
(6) Han, J.; Liu, T.; Hao, C.; Zhang, S.; Guo, B.; Zhang, J. *Macromolecules* **2018**, *51*, 6789–6799.
(7) Fortman, D. J.; Brutman, J. P.; Cramer, C. J.; Hillmyer, M. A.; Dichtel, W. R. *J. Am. Chem. Soc.* **2015**, *137*, 14019–14022.
(8) Zheng, N.; Hou, J.; Xu, Y.; Fang, Z.; Zou, W.; Zhao, Q.; Xie, T. *ACS Macro Lett.* **2017**, *6*, 326–330.
(9) Zheng, N.; Fang, Z.; Zou, W.; Zhao, Q.; Xie, T. *Angew. Chem. Int. Ed.* **2016**, *55*, 1–6.
(10) Chen, X.; Li, L; Jin, K.; Torkelson, J. *Polym. Chem.* **2017**, *8*, 6349–6355.
(11) Capelot, M.; Montarnal, D.; Tournilhac, F.; Leibler, L. *J. Am. Chem. Soc.* **2012**, *134*, 7664–7667.
(12) Rottger, M.; Domenech T.; van der Weegen, R.; Breuillac A.; Nicolay, R.; Leibler, L. *Science* **2017**, *356*, 62-65.
(13) Ogedn, W; Guan, Z. *J. Am. Chem. Soc.* **2018**, *140*, 6217–6220.
(14) Cromwell, R.; Chung, J.; Guan, Z. *J. Am. Chem. Soc.* **2015**, *137*, 6492–6495.
(15) Zheng, P.; McCarthy, T. J. *J. Am. Chem. Soc.* **2012**, 134, 2024–2027.

(16) Nishimura, Y.; Chung, J.; Muradyan, H.; Guan, Z. *J. Am. Chem. Soc.* **2017**, *139*, 14881–14884.
(17) Obadia, M. M.; Mudraboyina, B. P.; Serghei, A.; Montarnal, D.; Drockenmuller, E. *J. Am. Chem. Soc.* **2015**, *137*, 6078–6083.
(18) Taynton, P.; Yu, K.; Shoemaker, R. K.; Jin, Y.; Qi, H. J.; Zhang, W. *Adv. Mater.* **2014**, *26*, 3938–3942.
(19) Taynton, P.; Ni, H.; Zhu, C.; Yu, K.; Loob, S.; Jin,Y.; Qi, H. J.; Zhang, W. *Adv. Mater.* **2016**, *49*, 6277–6284.
(20) Denissen, W.; Rivero, G.; Nicolaÿ, R.; Leibler, R.; Winne, J. M.; Du Prez, F. E. *Adv. Func. Mater.* **2015**, *25*, 2451–2457.
(21) Denissen, W.; Droesbeke, M.; Nicolay, R.; Leibler, L.; Winne, J. M.; Du Prez, F. E. *Nat. Commun.* **2017**, *8*, 14857.
(22) Lessard, J. J.; Garcia, L. F.; Easterling, C. P.; Sims, M. B.; Bentz, K. C.; Arencibia, S.; Savin, D. A.; Sumerlin, B. S. *Macromolecules* **2019**, *52*, 2105–2111.
(23) Christensen, P. R., Scheuermann, A. M., Loeffler, K. E.; Helms, B. A. *Nat. Chem.* **2019**, *11*, 442–448.
(24) Froidevaux, V.; Negrell, C.; Caillol, S.; Pascault, J. P.; Boutevin, B. *Chem. Rev.* **2016**, *116*, 14181–14224.
(25) Shriner, R. L.; Todd, H. R. *Organic Syntheses, XV,* 14–16; 1935.
(26) Anbarasan, P.; Baer, Z. C.; Sreekumar, S.; Gross, E.; Binder, J. B.; Blanch, H. W.; Clark, D. S.; Toste, F. D. *Nature* **2012**, *491*, 235–239.
(27) Fox Jr, T. G.; Flory, P. J. *J. Appl. Phys.* **1950**, *21*, 581–591.
(28) Auvergne, R.; Caillol, S.; David, G.; Boutevin, B.; Pascault, J.-P. *Chem. Rev.* **2014**, *114*, 1082–1115.

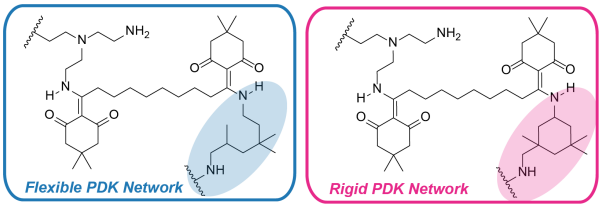
Flexible PDK Network
Rigid PDK Network

Supporting Information

for

Conformational Entropy as a Means to Control the Behavior of Poly(diketonenamine) Vitrimers In and Out of Equilibrium

Changfei He,[1] Peter R. Christensen,[2] Trevor J. Seguin,[3] Brandon M. Wood,[4,5] Kristin A. Persson,[5,6] Thomas P. Russell,[*,1,7,8] and Brett A. Helms[*,2,8]

[1]Beijing Advanced Innovation Center for Soft Matter Science and Engineering, Beijing University of Chemical Technology, Beijing 100029, China

[2]The Molecular Foundry, Lawrence Berkeley National Laboratory, 1 Cyclotron Road, Berkeley, California 94720, United States

[3]Energy Technologies Area, Lawrence Berkeley National Laboratory, 1 Cyclotron Road, Berkeley, California 94720, United States

[4]Graduate Group of Applied Science and Technology, University of California, Berkeley, California 94720, United States

[5]Environmental Energy Technologies Division, Lawrence Berkeley National Laboratory, 1 Cyclotron Road, Berkeley, California 94720, United States

[6]Materials Science and Engineering Department, University of California, Berkeley, California 94720, United States

[7]Polymer Science and Engineering Department, University of Massachusetts Amherst, Massachusetts 01003, United States

[8]Materials Sciences Division, Lawrence Berkeley National Laboratory, 1 Cyclotron Road, Berkeley, California 94720, United States

Correspondence: tom.p.russell@gmail.com and bahelms@lbl.gov

Materials

2,2,4(2,4,4)-Trimethyl-1,6-hexanediamine (THMDA, 99%), 5-amino-1,3,3-trimethylcyclohexanemethylamine as a mixture of *cis* and *trans* isomers (99%) (i.e., isophorone diamine, IPDA), 5,5-dimethyl-1,3-cyclohexanedione (95%), sebacic acid (99%), 4-(dimethylamino)pyridine (DMAP, 99%), *N,N'*-dicyclohexylcarbodiimide (DCC, 99%) were purchased commercially and used as received unless otherwise noted. Monomer TK-10 was synthesized as described by us previously.[1] All anhydrous solvents (EMD Millipore)—dichloromethane (DCM), benzene, methanol, ethyl acetate—were purchased and used without further purification.

General Synthesis of PDK Vitrimers. The linear segments of PDK vitrimers were initially synthesized in the melt (90 ˚C) from triketone monomer TK-10 (4.00 g, 8.96 mmol) and either TMHDA (312–936 mg, 1.97–5.91 mmol) or IPDA (336–1006 mg, 1.97–5.91 mmol). This reaction mixture was then crosslinked with TREN (1152–384 mg, 5.25–2.63 mmol). Resins were transferred to a vacuum oven (120 ˚C) for 12 h, after which time they could be molded or, alternatively, pulverized in a ball mill and subsequently molded. PDK **1** was networked with TREN only; PDKs **2**–**4** have TMHDA loadings of 20%, 40%, and 60%, respectively; PDKs **5**–**7** have IPDA loadings of 20%, 40%, and 60%, respectively. The amine excess in all PDK formulations was 10 mol%.

Methods

Solid-State Nuclear Magnetic Spectroscopy (NMR). ^{1}H–^{13}C cross polarization (CP) nuclear magnetic resonance spectra were collected on a 11 Tesla magnet at a ^{13}C frequency of 125.7 MHz under 10 kHz magic-angle spinning (MAS) condition. A Bruker 4 mm H/X probe and Bruker AV-500 spectrometer were used. The Hartmann–Hahn condition for CP experiments was obtained on solid adamantane, which was also used as a secondary reference for ^{13}C chemical shift (the methylene signal of adamantane was set to 38.48 ppm relative to TMS). Two-pulse phase modulation (TPPM) proton decoupling was used. The TPPM angle was 15 degrees and the decoupling field strength was ~50 kHz. A contact time of 0.5 ms and a pulse delay of 4 s were used in the CP experiments.

Solution-Phase NMR. ^{1}H and ^{13}C NMR spectra were recorded on Bruker Avance II at 500 Mz and 125 MHz, respectively. Chemical shifts are reported in δ (ppm) relative to the residual solvent peak ($CDCl_3$: 7.26 for ^{1}H, 77.16 for ^{13}C). Splitting patterns are designated as s (singlet), br s (broad singlet), d (doublet), t (triplet), q (quartet), and m (multiplet).

Differential Scanning Calorimetry (DSC). Data were acquired using a TA instruments Q200 Differential Scanning Calorimeter. Samples were heated 0–200 ˚C

at a rate of 10 °C min^{-1} under a N_2 atmosphere. For each sample, data acquisition runs consisted of a heating step, a cooling step, and a second heating step. Glass transition temperatures (T_g) were interpreted and reported from the second heating curve.

Thermogravimetric Analysis (TGA). Data were acquired using a TA instruments TGA 5500. Samples were heated 25–600 °C under an air atmosphere at a rate of 10 °C min^{-1}.

Fourier Transform Infrared Spectra (FTIR). Data were acquired using a Perkin Elmer Spectrum One spectrophotometer as an average of 25 scans over an energy range of 600–4000 cm^{-1}. A ZnSe ATR accessory was used for analyzing PDK films.

Dynamic Mechanical Analysis (DMA). Data were acquired using a TA instruments DMA Q800 in tensile film mode. All samples were fabricated as rectangular specimens with ~ 0.5 mm (T) × 5 mm (W) × 20 mm (L). Each were tested at a frequency of 1 Hz and a strain of 0.12%. Heating ramps of 3 °C min^{-1} were applied from 30–150 °C. The glass transition temperature (T_g) was reported as the maximum value of tan δ.

Cross-linking density (ν) and molecular weight between cross-links (M_x) were calculated from equation (1):[1]

$$E' = 3\nu RT = \frac{3\rho RT}{M_x} \qquad (1)$$

where E' is the modulus of the rubbery plateau determined by DMA, ν is cross-linking density, ρ is the density of the PDK vitrimer, R is the gas constant, and T refers to the absolute temperature (373 K).

Stress Relaxation Analysis (SRA). Data were acquired using a TA DMA Q800 instrument. SRA was conducted using rectangular specimens ~ 0.5 mm (T) × 5 mm (W) × 20 mm (L). SRA experiments were performed under strain control at a constant temperature (120–180 °C). Samples were allowed to equilibrate at this temperature for approximately 5 min. A constant, normal strain of 0.1% was applied to each sample, prior to subjecting it to an instantaneous strain of 1%. The stress decay was monitored, while maintaining a constant strain (1%). The relaxation modulus (G) was normalized by initial value (G_0). The characteristic relaxation time (τ^*) was defined as the time required for $G/G_0 = 1/e$ with exponential decay function: $G(t) = G_0 \exp(-t/\tau^*)$.

We further implemented SRA to determine the topology freezing transition temperature (T_v) for PDK vitrimers.[3] T_v is defined as the temperature at which the material reaches a viscosity of 10^{12} Pa·s. The viscosity η and characteristic relaxation time τ are related via the Maxwell relation, equation (3):

$$\eta = G \cdot \tau = \frac{E'}{2(1+\nu)} \cdot \tau \qquad (3)$$

where G is the shear modulus, ν is the Poisson's ratio and E' is the storage modulus at the rubbery plateau. Assuming a Poisson's ratio = 0.5, equation (3) reduces to equation (4):

$$\eta = \frac{\tau \cdot E'}{3} \qquad (4)$$

At the same time relaxation time τ were fitted to the Arrhenius equation (5),

$$\ln \tau(T) = \ln \tau_0 + E_a / RT \qquad (5)$$

where E_a is the activation energy for solid-state associative bond exchange as determined by SRA. As η = 10^{12} Pa s, combining eq (4) and eq (5) then we arrive at eq (6):

$$\ln(\frac{3\times10^{12}}{E'}) = \ln \tau_0 + E_a / RT_v \qquad (6)$$

From eq (6), the T_v was determined.

Tensile Tests. Tensile tests were performed on Instron 3345 tensile instrument using dog-bone samples according to the ASTM-628 standard (dimension of narrow portion is 10 mm (L) × 3 mm (W) × 1 mm (T)) with a strain rate of 5 mm min^{-1}. Data are reported as the average from at least 3 samples.

Tensile strength at temperatures greater than the sample's T_g were determined by DMA by using a constant force mode, using rectangular specimens ~ 0.5 mm (T) × 5 mm (W) × 20 mm (L). Samples were heated above their T_g and equilibrated at that temperature for 5 min. They were then subjected to a controlled force of 3 N min^{-1}.

Swelling Tests. Swelling experiments were performed by soaking samples in 20 mL benzene at 20 ˚C for 24 h. After removing the solvent and washing the sample with methanol, the samples were finally dried in vacuo at 120 ˚C. The gel fraction was calculated using equation (2)

$$Gel\% = \frac{m_{dry}}{m_{initial}} \times 100\% \qquad (2)$$

Where $m_{initial}$ is the original weight the sample, m_{dry} is weight of samples after drying from the solvent.

Theoretical Methods. All calculations were carried out using Gaussian 16[4] with the PM7 method.[5] To generate the torsional scans (Figure 4), a conformation search was first performed on the two monomers to locate their global energy minima. An initial set of relaxed dihedral scans were performed for each structure on all the bonds indicated over 360 degree rotations in increments of 6 degrees in both directions. From this scan, structures were obtained at steps corresponding to 72, 144, 216 and

288 degree rotations in one direction and conformation searches were performed to find the minimum energy conformation at these steps with respect to all other bonds (i.e., the rotation of the bond involved in the dihedral angle scan was held fixed). Then relaxed dihedral angle scans were performed on these conformations over 360 degrees in 6 degree increments in both directions for the bond that was previously scanned. This led to ten torsional angle scans for each of the bonds (Figure 4). This data was converted to that of 1 degree increments using linear interpolation. For each bond, the lowest energy was taken at each step of rotation from their respective set of ten torsional potential energy curves to obtain the final torsional potential energies given. This data contained sharp bends and kinks along some of torsional scans that reflected abrupt flexion of the molecule outside of the bond involved in the torsional scan. Therefore, the data was smoothed using locally weighted scatterplot smoothing[6] with a smoothing parameter of 0.05 to generate the plots reported in Figure 4.

Partition functions reported in Figure 1b were computed based on the torsional potentials at all points for every bond for each monomer using:

$$q = \sum_i \frac{\Delta E_i}{k_B T},$$

where ΔE is the energy relative to the global minimum, k_B is the Boltzmann constant and T is temperature.

Supporting Figures

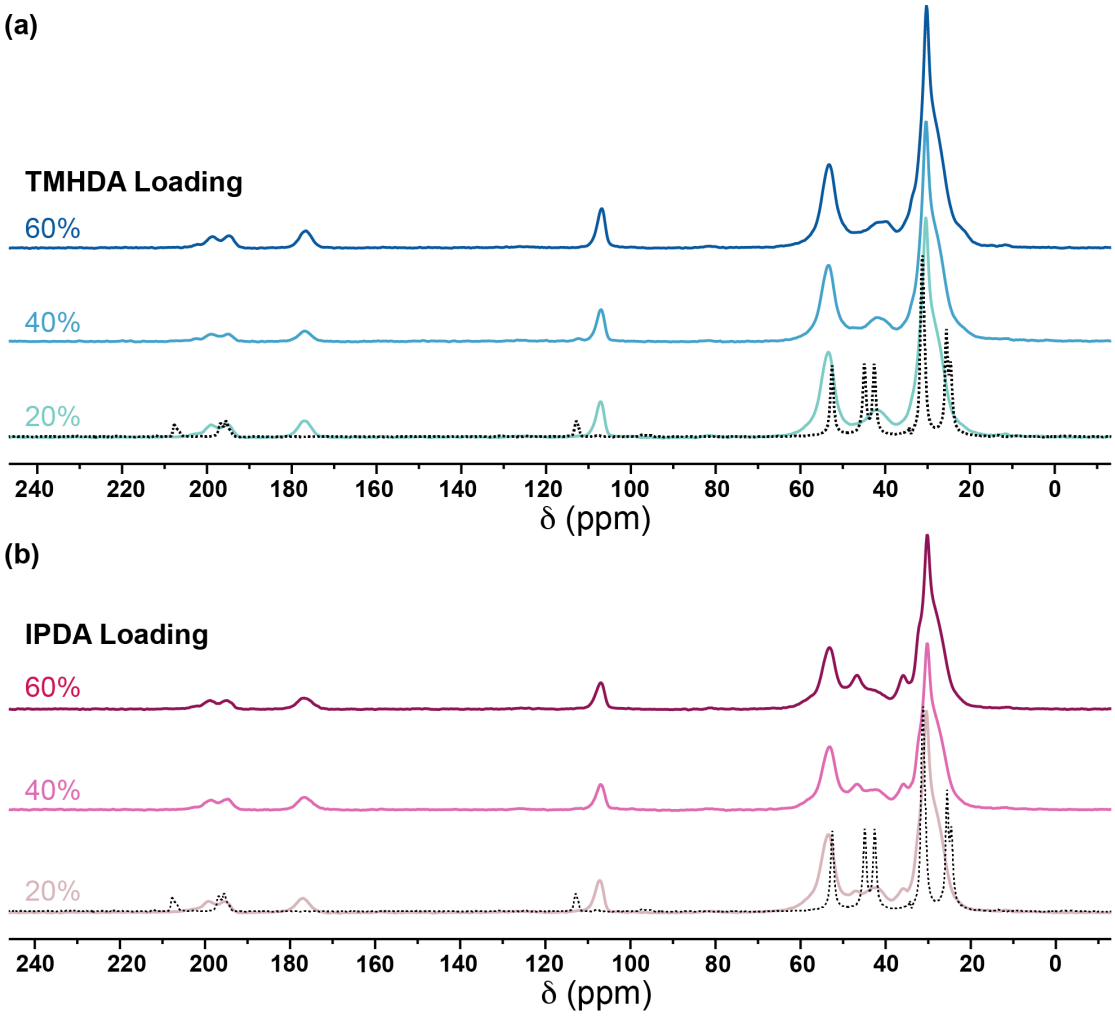

Figure S1. Solid-state ^{1}H–^{13}C cross polarization NMR spectra of (a) TMHDA-based PDK vitrimers **2**–**4**, and (b) IPDA-based vitrimers **5**–**7**. The black dashed line indicates the monomer TK-10.

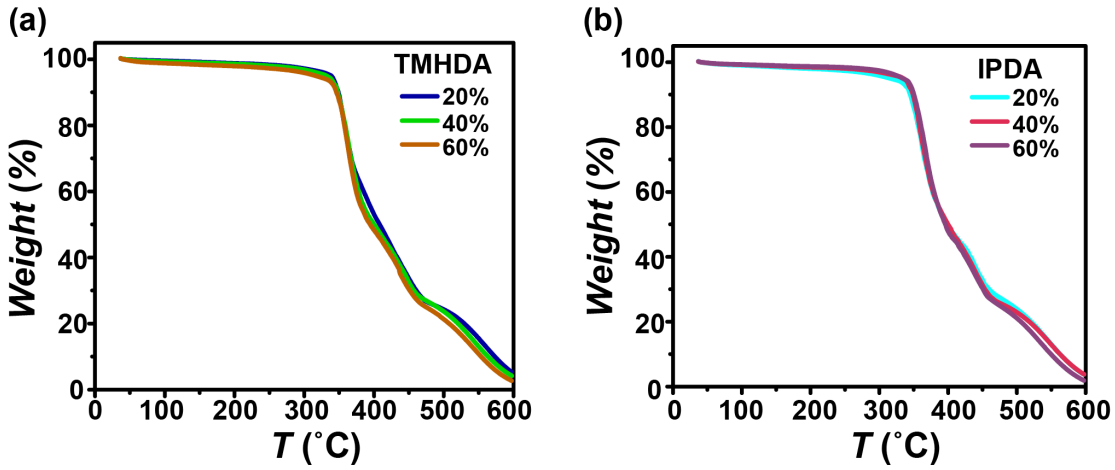

Figure S2. TGA of PDK vitrimers incorporating either (a) TMHDA- or (b) IPDA -based linear segments of varying molecular weight.

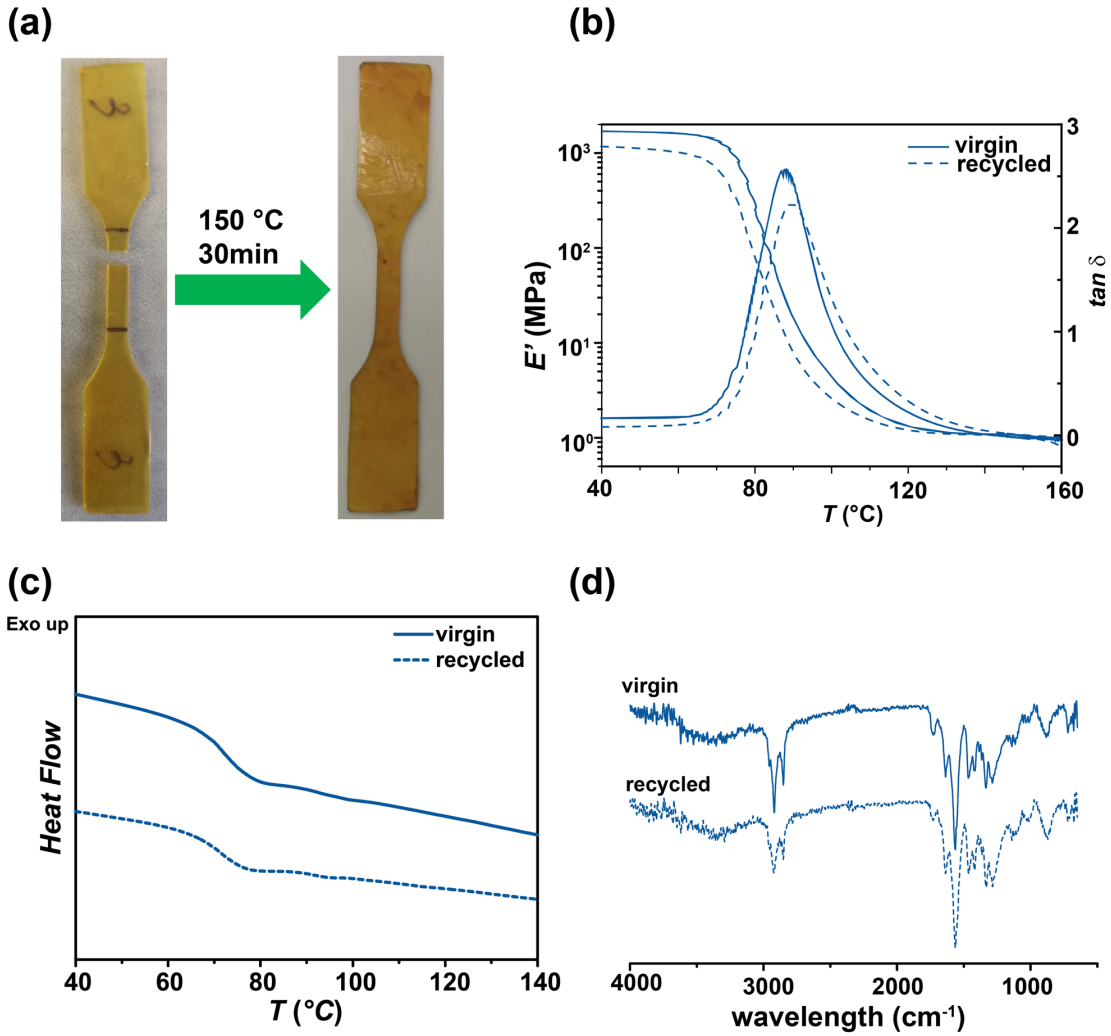

Figure S3. (a) Compression-molded PDK **4** (60% THMDA loading) after having been broken into two two pieces during a tensile test, and after being reprocessed and repaired. (b) DMA curves of virgin and recycled PDK **4**. (c) DSC curves of virgin and recycled PDK **4**. (d) ATR-FTIR spectra of virgin and recycled PDK **4**.

Table S1. Gel fraction of PDK vitrimers.

Sample	Initial Mass (mg)	Final Mass (mg)	gel fraction (%)
PDK **2**	113.3	109.6	97
PDK **3**	169.0	160.3	95
PDK **4**	158.6	150.3	95
PDK **5**	214.3	210.1	98
PDK **6**	156.4	146.8	94
PDK **7**	141.2	132.2	93

Table S2. Thermal mechanical properties of PDK vitrimers

Sample	T_g (˚C) by DSC	T_g (˚C) by DMA	*E'* in the glassy state (MPa)	*E'* in the rubbery state[a,b] (MPa)	ρ (g cm^{-3})	ν (mol cm^{-3})	*M*W (kg mol^{-1})
PDK **2**	88	100	1350	2.5	0.92	2.4×10^{-4}	3.8
PDK **3**	78	92	1350	1.5	0.92	1.5×10^{-4}	6.3
PDK **4**	71	85	1200	1.0	0.93	9.7×10^{-5}	9.6
PDK **5**	105	122	1450	2.6	0.98	2.3×10^{-4}	4.3
PDK **6**	110	130	1350	1.4	0.96	1.2×10^{-4}	7.8
PDK **7**	117	138	1350	0.94	0.99	8.3×10^{-5}	11.9

a E' determined at 140 ˚C by DMA for TMHDA-based PDK vitrimers **2**–**4**.
b E' determined at 180 ˚C by DMA for IPDA-based PDK vitrimers **5**–**7**.

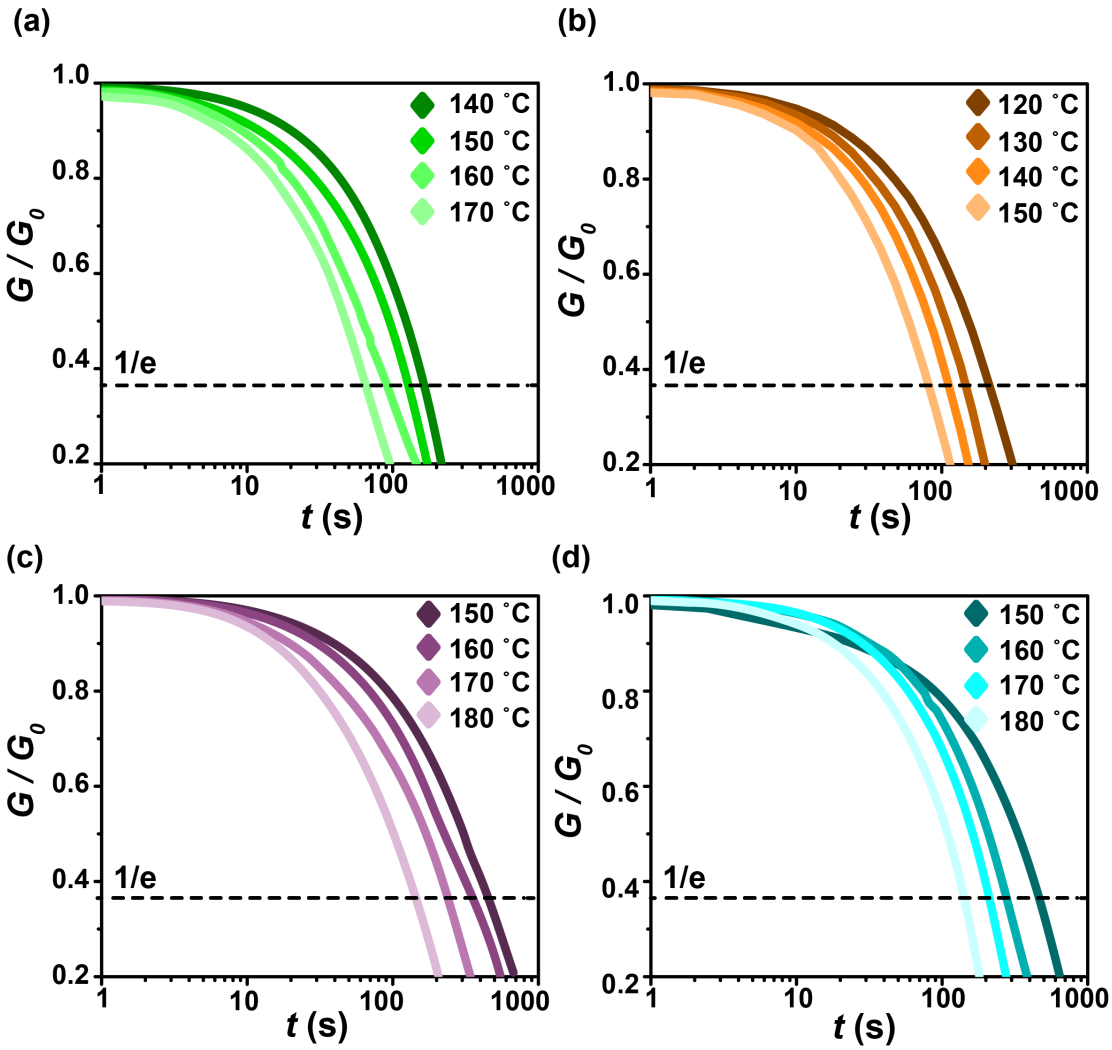

Figure S4. Normalized stress-relaxation curves at different temperatures for (a) PDK **3**, (b) PDK **4**, (c) PDK **6,** and (d) PDK **7**. The dash line indicates 37% of G_0. Data were acquired at 1% strain.

Table S3. T_v values for PDK vitrimers

Sample	PDK **2**	PDK **3**	PDK **4**	PDK **5**	PDK **6**	PDK **7**
T_v (°C)	−20	−30	−45	−1	9	11

Table S4. Mechanical properties of PDK vitrimers

Sample	*Young's Modulus* (MPa)	*Stress at break* (MPa)	*Strain at break* (%)
PDK **2**	1790 ± 85	23.0 ± 3.4	1.2 ± 0.13
PDK **3**	1721 ± 64	29.6 ± 2.8	1.7 ± 0.19
PDK **4**	1711 ± 49	33.0 ± 7.2	1.9 ± 0.47
PDK **4** (recycled)	1828 ± 118	31.0 ± 4.4	0.18 ± 0.19
PDK **5**	1920 ± 132	19.2 ± 3.1	1.0 ± 0.17
PDK **6**	1662 ± 167	19.1 ± 1.7	1.2 ± 0.13
PDK **7**	1417 ± 70	18.6 ± 1.1	1.3 ± 0.15

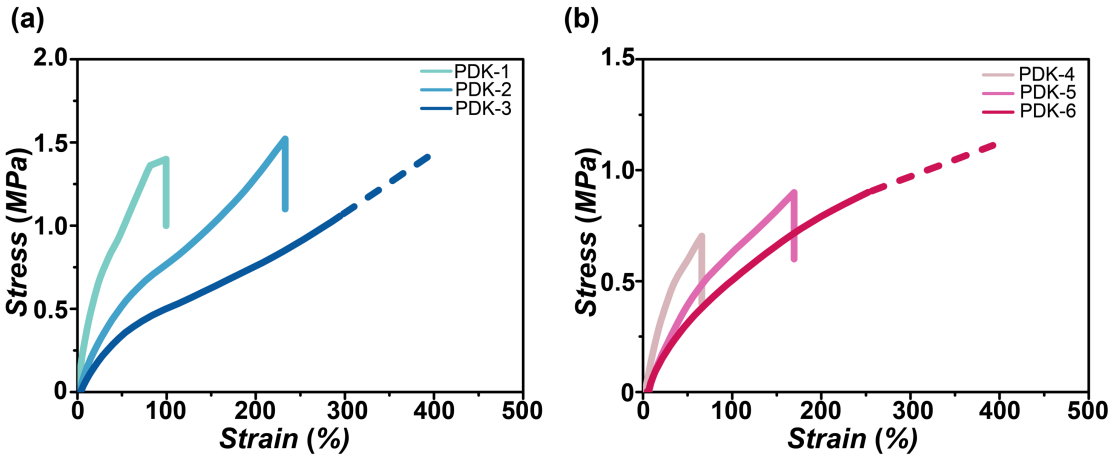

Figure S5. Stress-strain curves at temperatures above the T_g of (a) TMHDA-based PDK vitrimers (T = 100 ˚C) and (b) IPDA-based PDK vitrimers (T = 140 ˚C).

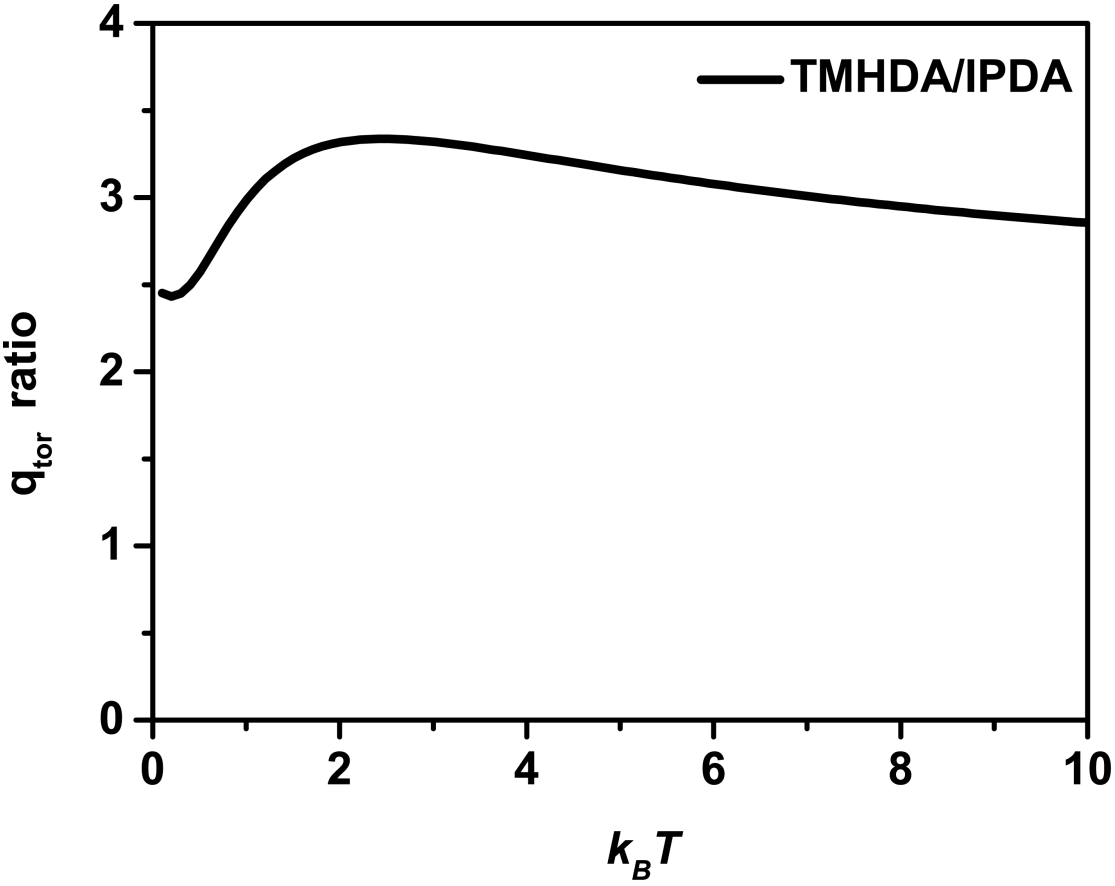

Figure S6. Quantifying the ratio of the torsional partition functions q_{tor} for molecular models of TMHDA- and IPDA-derived PDK monomer segments as a function. It is significant that the ratio exceeds 7/3, which is the number of rotatable bonds in each model compound, in that it indicates more rotational degrees of freedom for TMHDA-based than for IPDA-based monomer segments.

Supporting References

1. David Roylance. Engineering viscoelasticity. **2011**, 8–11
2. Christensen, P. R., Scheuermann, A. M., Loeffler, K. E.; Helms, B. A. *Nat. Chem.* **2019**, 11, 442–448.
3. Denissen, W.; Rivero, G.; Nicolaÿ, R.; Leibler, R.; Winne, J. M.; Du Prez, F. E. *Adv. Func. Mater.* **2015**, *25*, 2451–2457.
4. Frisch, M. J.; Trucks, G. W.; Schlegel, H. B.; Scuseria, G. E.; Robb, M. A.; Cheeseman, J. R.; Scalmani, G.; Barone, V.; Petersson, G. A.; Nakatsuji, H.; Li, X.; Caricato, M.; Marenich, A. V.; Bloino, J.; Janesko, B. G.; Gomperts, R.; Mennucci, B.; Hratchian, H. P.; Ortiz, J. V.; Izmaylov, A. F.; Sonnenberg, J. L.; Williams; Ding, F.; Lipparini, F.; Egidi, F.; Goings, J.; Peng, B.; Petrone, A.; Henderson, T.; Ranasinghe, D.; Zakrzewski, V. G.; Gao, J.; Rega, N.; Zheng, G.; Liang, W.; Hada, M.; Ehara, M.; Toyota, K.; Fukuda, R.; Hasegawa, J.; Ishida, M.; Nakajima, T.; Honda, Y.; Kitao, O.; Nakai, H.; Vreven, T.; Throssell, K.; Montgomery Jr., J. A.; Peralta, J. E.; Ogliaro, F.; Bearpark, M. J.; Heyd, J. J.; Brothers, E. N.; Kudin, K. N.; Staroverov, V. N.; Keith, T. A.; Kobayashi, R.; Normand, J.; Raghavachari, K.; Rendell, A. P.; Burant, J. C.; Iyengar, S. S.; Tomasi, J.; Cossi, M.; Millam, J. M.; Klene, M.; Adamo, C.; Cammi, R.; Ochterski, J. W.; Martin, R. L.; Morokuma, K.; Farkas, O.; Foresman, J. B.; Fox, D. J. *Gaussian 16 Rev.* B.01, Wallingford, CT, 2016.
5. Stewart, J. J. P. *J. Mol. Model.* **2013**, *19*, 1–32.
6. Cleveland, W. S. *J. Am. Stat. Assoc*. **1979**, 74, 829-836.